COMPLEX MODE CALCULATION BY FINITE ELEMENT METHOD

COMPLEX MODE CALCULATION BY FINITE ELEMENT METHOD

BY

TINGXIA LI, B.Sc.

A THESIS

SUBMITTED TO THE DEPARTMENT OF ELECTRICAL & COMPUTER ENGINEERING

AND THE SCHOOL OF GRADUATE STUDIES

OF MCMASTER UNIVERSITY

IN PARTIAL FULFILMENT OF THE REQUIREMENTS

FOR THE DEGREE OF

MASTER OF APPLIED SCIENCE

Master of Applied Science (2012) McMaster University

(Electrical & Computer Engineering) Hamilton, Ontario, Canada

TITLE:	COMPLEX MODE CALCULATION BY FINITE ELEMENT METHOD
AUTHOR:	TINGXIA LI B.Sc., (Electrical Engineering) University, City, Country
SUPERVISOR:	Dr. Wei-Ping Huang
NUMBER OF PAGES:	xii, 60

Abstract

Optical waveguide is a very important component in numerous optical structures, devices and photonic circuits. With the rapid development of fabrication technologies, increasing integrated complexity and different materials characteristics, there is higher demand on high-index contrast waveguide with arbitrary cross section and anisotropic material, which indicates the need to develop an efficient, high-performance mode solver to analyze optical waveguides to reduce the fabrication cycle and total cost. Modeling and simulation methods, including Finite Difference Time-Domain (FDTD) method, Finite Element Method (FEM), Beam Propagating Method (BPM), Mode Matching Method (MMM) and Couple Mode Theory (CMT), etc, have been popular for years. Among those methods, FEM is a good and efficient method, especially for its superiority on arbitrary meshes.

In this thesis, both scalar and vectorial FEM mode solvers are implemented with an emphasis on dealing with the radiation and evanescent modes by enclosing the whole region with the Perfect Matched Layer (PML) and Perfect Reflecting Boundary (PRB). Thus, the unbounded and continuous radiation modes together with evanescent modes are replaced by what we called "complex modes", but still keeping the completeness and orthogonality properties.

Acknowledgements

A great deal of thanks is owed to Dr. Wei-Ping Huang for his supervision on this Master's Thesis. His continued support and guidance, combined with his understanding encouragement and endless patience is greatly appreciated. His rich knowledge, energetic mind and grand vision would have continuous and lasting positive influence on me.

I also would like to give my thanks to Dr. Xun Li, Dr. Patricu for their teaching and assistance. And to Dr. Bakr for his help and advice.

Additional thanks to Lin Han for sharing his experience and providing help and advice when needed even when he is extremely busy.

Thank to Lanxin Deng, Xiaojun Liang, Yefeng Wen, Jing Shao, Haibo Liang, Yunfei Cai for their support and friendship, which I would value for the rest of my life.

Special thanks to my parents for their love and support financially and mentally. Without them I am nothing in this world. And to my fiance, Xishi Dai, for his endless support and love.

Notation and Abbreviations

2D	two-dimensional
3D	three-dimensional
BC	Boundary Condition
BVP	Boundary-Value Problem
CMT	Coupled Mode Theory
FDM	Finite Different Method
FDTD	Finite Different in Time Domain
FEM	Finite Element Method
LP	Linearly Polarized
PML	Perfectly Matched Layer
PRB	Perfectly Reflecting Boundary
SFEM	Scalar Finite Element Method

Contents

List of Tables

List of Figures

Chapter 1

Introduction

1.1 Background and Motivation

1.1.1 Problems and Methods

Boundary-value problems (BVPs) have been a major topic in the physics and mathematics simulation in a variety of areas such as thermal, mechanical, electrical, magnetic and fluid flow. For many boundary-value problems, a mathematical model can be extracted, resulting in one or a group of related algebraic, differential or/and integral equations [1], and in most of the cases, differential equations.

However, finding a analytical solution which satisfies the differential equations as well as the boundary condition in the entire region is often difficult if not impossible in most of the circumstances except for the very simple cases. In practice, one seek numerical solutions by approximating the governing equations by expanding the solution in terms of some qualified base functions and/or discretizing the equations by certain numerical schemes. With the development of computer-aid design (CAD) in

recent decades, the latter is becoming more and more popular, accurate and faster. In this thesis, we will concentrate on the eigenvalue problems related to the modal solutions in three-dimension(3D) straight optical waveguides with two-dimension (2D) cross sections.

There are a number of available methods and techniques which can solve the eigenvalue problems numerically, such as the finite element method (FEM), the finite difference method (FDM), the mode matching method (MMM),etc[2].

The Finite Element Method [3], which I will present in this thesis, is a widely used numerical technique for obtaining rigorous solutions to boundary-value problems.

1.1.2 Introduction to Finite Element Method

Starting from aircraft structure, the Finite Element Method (FEM) has been widely used in the past 40 years in different disciplines and specializations including electromagnetic problems. A broad definition of FEM is given as [1]:

The Finite Element Method is a computer-aided mathematical technique for obtaining approximate numerical solutions to the abstract equations of calculus that predict the response of physical systems subjected to external influences.

Similar to other numerical solution techniques, the finite element method divides an entire region into small subregions so that one can obtain an approximate solution within each subregion that satisfies the boundary conditions of the adjacent subregions. And within each subregion, the simpler solution can be derived compared with the entire region.

In the earlier decades of FEM's application in waveguides and antennas, it is restricted because of the so-called spurious solutions in vectorial FEM, which are false mode solutions. Recently, the introduction of edge elements has solves this problems successfully. FEM sees a revival since then with the revolution in computer hardware and software.

1.2 Introduction to Perfectly Mached Layer

1.2.1 Why PML

The set of Maxwell Equations is the very basic governing equation for waveguides. However in open waveguides, the boundary is in fact the boundless infinite space theoretically which makes it impossible to solve by discretization only. What's more, the computation region that we are interested in is actually limited in the waveguide cross-section. And the modes in open waveguides are classified into three groups: the guided modes, the radiation modes and the evanescent modes, with discretized, real propagation constant, continuous, real propagation constant and continuous, imaginary constant, respectively. However, these "real" values have some restrictions while applied into reality: the unbounded mode field of radiation mode can't not be normalized in normal way but in terms of Dirac delta function; the continuity of the propagation constant limits its application in many mode-based method, such as Coupled Mode Theory (CMT) and Mode Matching Method (MMM).

In following chapters, we use the Perfectly Reflecting Boundary (PRB) condition and it's size is restrained, which is good and has been used for years. The modes then are reduced to discretized and bounded solutions which can be classified into

the guided modes, the box modes and the evanescent modes. This technique is a good approximation while the dimension of the guiding region is much small than that of the box, but due to the PRB, there is always reflection on the boundary. As the power constrained in the core gets lower, the reflection is becoming more and more significant, especially for the box modes and evanescent modes.

Another drawback is that box modes and evanescent modes depend on the box size critically, including the number of modes and the spacing between two modes.

Nevertheless, this problem still could be solve by applying special boundary conditions in order to absorb the outgoing waves, such as techniques like radiation boundary which is popular in the 70's last century, and the "matched layer" which consists of an absorbing medium surrounding the computation domain, whose impedance matches those of the free space, etc. However, these techniques have their limits, such as some only suitable for specific cases: propagation on specific direction, in a specific frequency, a thick boundary which increases the computation nodes, etc. Thus we introduce the Perfectly Matched Layer as the boundary condition in this FEM technique.

1.2.2 What is PML

The perfectly matched layer is a non-physical fictitious medium that is used to anti-reflectively match a real physical medium, and attenuates the incident waves of any frequency and at any incidence angle without reflection theoretically. This is proved by Berenger in 1994 [4].

1.3 Organization of Thesis

In this thesis, we will first give a basic introduction to the theory of FEM, then we will derive and validate the scalar FEM and vectorial FEM.

For detail, in chapter 2, the governing equation, including the set of maxwell equations, modified maxwell equations with coordinate stretching method are presented.

In chapter 3, theory and basic FEM methods and steps will be given.

In chapter 4, a Scalar FEM (SFEM) formulation in inhomogeneous waveguide is derived and applied to waveguides of arbitrary transverse shape. The examples of a rectangular dieletric waveguide, a circular waveguide and a ridge waveguide are presented and analyzed to validate the Scalar FEM with boundary condition of Perfectly Reflecting Boundary (PRB) and Perfectly Matched Layer (PML) boundary condition.

In chapter 5, an edge-based Full-Vectorial FEM (VEFM) is introduced with two-dimensional edge elements for analyzing inhomogeneous waveguide. And same examples are presented to validate the method and the orthogonality property is analyzed.

Chapter 2

Governing Equations

2.1 Maxwell Equations

Differential form of Maxwell equations is shown as

$$\nabla \times \mathbf{E} = -j\omega\hat{\mu}\mathbf{H} \tag{2.1}$$

$$\nabla \times \mathbf{H} = j\omega\hat{\epsilon}\mathbf{E} \tag{2.2}$$

$$\nabla \cdot (\hat{\epsilon}\mathbf{E}) = 0 \tag{2.3}$$

$$\nabla \cdot (\hat{\mu}\mathbf{H}) = 0 \tag{2.4}$$

where $\mathbf{E}$ and $\mathbf{H}$ are the phsor expressions and $\hat{\epsilon} = \epsilon_0\hat{\epsilon}_r$, $\hat{\mu} = \mu_0\hat{\mu}_r$. $\hat{\epsilon}_r$ and $\hat{\mu}_r$ may be tensors (tenser a denoted as $\hat{a}$ or [a] in this thesis) in anisotropic medium. Substitute (2.1) into (2.2), and (2.2) into (2.1) we have the curl-curl equations as

$$\nabla \times (\frac{1}{\hat{\mu}_r}\nabla \times \mathbf{E}) - k_0^2\hat{\epsilon}_r\mathbf{E} = 0 \tag{2.5}$$

and

$$\nabla \times (\frac{1}{\hat{\epsilon}_r}\nabla \times \mathbf{H}) - k_0^2 \hat{\mu}_r \mathbf{H} = 0 \tag{2.6}$$

where $k_0^2 = \omega^2 \epsilon_0 \mu_0$. Equation (2.5) and (2.6) may be written as (2.7)

$$\nabla \times ([p]\nabla \times \mathbf{\Phi}) - k_0^2 [q]\mathbf{\Phi} = 0 \tag{2.7}$$

where

$$\mathbf{\Phi} = (\Phi_x \hat{x} + \Phi_y \hat{y} + \Phi_z \hat{z})\exp(-j\beta z) \tag{2.8}$$

and

$$[p] = \frac{1}{\hat{\mu}_r} = \begin{pmatrix} 1/\mu_{xx} & 1/\mu_{xy} & 1/\mu_{xz} \\ 1/\mu_{yx} & 1/\mu_{yy} & 1/\mu_{yz} \\ 1/\mu_{zx} & 1/\mu_{zy} & 1/\mu_{zz} \end{pmatrix}, [q] = \hat{\epsilon}_r = \begin{pmatrix} \epsilon_{xx} & \epsilon_{xy} & \epsilon_{xz} \\ \epsilon_{yx} & \epsilon_{yy} & \epsilon_{yz} \\ \epsilon_{zx} & \epsilon_{zy} & \epsilon_{zz} \end{pmatrix} \tag{2.9}$$

for $\mathbf{\Phi} = \mathbf{E}$, and

$$[p] = \frac{1}{\hat{\epsilon}_r} = \begin{pmatrix} 1/\epsilon_{xx} & 1/\epsilon_{xy} & 1/\epsilon_{xz} \\ 1/\epsilon_{yx} & 1/\epsilon_{yy} & 1/\epsilon_{yz} \\ 1/\epsilon_{zx} & 1/\epsilon_{zy} & 1/\epsilon_{zz} \end{pmatrix}, [q] = \hat{\mu}_r = \begin{pmatrix} \mu_{xx} & \mu_{xy} & \mu_{xz} \\ \mu_{yx} & \mu_{yy} & \mu_{yz} \\ \mu_{zx} & \mu_{zy} & \mu_{zz} \end{pmatrix} \tag{2.10}$$

for $\mathbf{\Phi} = \mathbf{H}$.

Equation (2.7) is the vector three component wave equation without any approximation.

2.1.1 Vector Mode Equations

If we separate the field into transverse and longitudinal direction components $\mathbf{\Phi} = \mathbf{\Phi}_t + \mathbf{\Phi}_z$ with (2.8) in isotropic and non-magnetic (i.e. $\hat{\epsilon}_r = \epsilon_r, \hat{\mu}_r = \mu_r = 1$) medium, we have the vector mode equations (2.11) and (2.12) for the transverse fields.

$$\nabla_t^2 \mathbf{E_t} + (n^2 - n_{eff}^2)k^2 \mathbf{E_t} = -\nabla_t \frac{1}{n^2}(\nabla_t n^2 \cdot \mathbf{E_t}) \tag{2.11}$$

$$\nabla_t^2 \mathbf{H_t} + (n^2 - n_{eff}^2)k^2 \mathbf{H_t} = -\frac{1}{n^2}\nabla_t n^2 \times (\nabla_t \times \mathbf{H_t}) \tag{2.12}$$

where n_{eff} is the effective refractive index and $n_{eff}\beta = k$ where β is the propagation constant and k the wave number. And the coupling between $\mathbf{E_t}$ and $\mathbf{H_t}$ are given as (2.13) and (2.14)

$$\mathbf{E_t} = \frac{Y_0 n^2}{n_{eff}} \hat{z} \times \mathbf{H_t} - \frac{Y_0}{n_{eff} k^2} \hat{z} \times [\nabla_t \times (\nabla_t \times \mathbf{H_t})] \tag{2.13}$$

$$\mathbf{H_t} = -\frac{Z_0}{n_{eff}} \hat{z} \times \mathbf{E_t} + \frac{Z_0}{n_{eff} k^2} \hat{z} \times [\nabla_t \times \frac{1}{n^2}(\nabla_t \times \mathbf{E_t})] \tag{2.14}$$

2.1.2 Semi-vector Mode Equations

In most of the cases, one of the polarization directions of the $\mathbf{E_t}$ field or $\mathbf{H_t}$ field in the full vector modes is much larger than the other one. Under this circumstance, the cross-coupling terms in (2.11) and (2.12) can be neglected. Consequently, the hybrid full vector modes, often referred to as quasi Transverse Electric (TE) modes and quasi Transverse Magnetic (TM) modes, are reduced to pure TE and pure TM modes. This approximation is referred as the semi-vector approximation.

2.1.3 Scalar Mode Equations

In Semi-vector approximation, the transverse field has two polarizations, TE and TM. The modes associated with the two polarization have different field profiles and mode effective refractive index. If the refractive index discontinuity is very small ($\delta n \approx 0$), the wave equations can be further reduced into the scalar wave equation with potential ϕ as (2.15) and the polarization dependence between the TE and TM modes vanishes and the mode effective refractive index become degenerate.

$$\nabla_t^2 \phi + k^2 \phi = 0 \tag{2.15}$$

2.2 Modified Maxwell Equations

The PML layer is a non-physical fictitious medium and can be regarded as artificial anisotropic media where $\hat{\epsilon} = \epsilon_0[\Lambda]$, $\hat{\mu} = \mu_0[\Lambda]$

A formulation similar to what is used by Berenger [4] is used in this thesis which is derived using coordinate stretching approach in [5]. A set of modified Maxwell equations of differential form are as below

$$\nabla_e \times \mathbf{E} = -j\omega\hat{\mu}\mathbf{H} \tag{2.16}$$

$$\nabla_h \times \mathbf{H} = j\omega\hat{\epsilon}\mathbf{E} \tag{2.17}$$

$$\nabla_h \cdot (\hat{\epsilon}\mathbf{E}) = 0 \tag{2.18}$$

$$\nabla_e \cdot (\hat{\mu}\mathbf{H}) = 0 \tag{2.19}$$

where

$$\nabla_e = \hat{x}\frac{1}{\alpha_{ex}}\frac{\partial}{\partial x} + \hat{y}\frac{1}{\alpha_{ey}}\frac{\partial}{\partial y} + \hat{z}\frac{1}{\alpha_{ez}}\frac{\partial}{\partial z} \tag{2.20}$$

$$\nabla_h = \hat{x}\frac{1}{\alpha_{hx}}\frac{\partial}{\partial x} + \hat{y}\frac{1}{\alpha_{hy}}\frac{\partial}{\partial y} + \hat{z}\frac{1}{\alpha_{hz}}\frac{\partial}{\partial z} \tag{2.21}$$

where α_{ep} and α_{hp}, $p = x, y, z$ are coordinate-stretching variables that stretch the x,y,z coordinates for ∇_e and ∇_h. And zero-reflection, i.e. the matching condition is

$$\alpha_{ep} = \alpha_{hp} = \alpha_p, \ p = x, y, z \tag{2.22}$$

where

$$\alpha_p = 1 \qquad \text{non-PML region} \tag{2.23}$$

$$\alpha_p = 1 - j\frac{\sigma_p}{\omega_0 \epsilon_0 n_{PMLp}^2} \qquad \text{PML region} \tag{2.24}$$

and α_p is called the complex coordinate-stretching factor and σ_p the electric or magnetic conductivity in p direction $p = x, y, z$ and in non-PML region, $\sigma_p = 0$.

The coordinate stretching method is equivalent to treating PML as special anisotropic medium but could be easily implemented and understood. Thus in this thesis, PML is implement with stretching coordinate methods.

Chapter 3

Finite Element Method Theory

3.1 Boundary Value Problems

A typical BVP can be defined by a governing differential equation in domain together with the boundary conditions on the boundary as (3.1).

$$\mathscr{L}\Phi = f \tag{3.1}$$

where L is a differential operator and f if the excitation and Φ is the unknown quantities. The Boundary Condition (BC) may be the simple Dirichlet (or first-type)(3.2), Neuman (second-type)(3.3), or hybrid boundary conditions, such as mixed Dirichlet and Neuman condition as shown in Figure (3.1), Robin conditions(impedance conditions, third-type)(3.4), or the complicated radiation conditions.

$$\Phi \mid_r = \Phi_0 \tag{3.2}$$

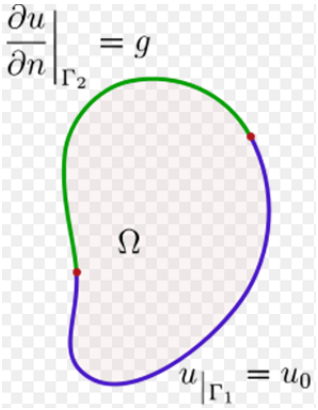

Figure 3.1: Mixed Dirichlet and Neuman boundary condition

$$\frac{\partial \Phi}{\partial n} \mid_r = g_0 \tag{3.3}$$

$$(a\Phi + b\frac{\partial \Phi}{\partial n}) \mid_r = g_0 \tag{3.4}$$

Most of the problems do not have an analytical solution for the unpredictable shape and material characteristics.

3.2 Methods

3.2.1 The Ritz Method

The Ritz method is a variational method in which the BVP of the form (3.1) is formulated in terms of a variational expression called functional $F(\Phi)$. The minimum of this functional corresponds to the governing differential equation under the given boundary conditions. In [6], Mikhlin proves that if the operator $\mathscr{L}$ in (3.1) is self-adjoint and positive definite, then the solution of (3.1) could be obtained by minimizing the functional (3.5)

$$F(\hat{\Phi}) = 0.5 < \mathscr{L}\hat{\Phi}, \hat{\Phi} > -0.5 < \hat{\Phi}, f > -0.5 < f, \hat{\Phi} > \tag{3.5}$$

where $< g, f >$ is the inner product of function g and f. For details, please refer to [6]. Once the functional is found, the solution can be obtained by the procedure described below. For simplicity, let us assume that the problem is real-valued. Suppose that $\hat{\Phi}$ in (3.5) can be approximated by the expansion (3.6)

$$\hat{\Phi} = \sum_{j=1}^{N} c_j v_j = \vec{c}^T \vec{v} = \vec{v}^T \vec{c} \tag{3.6}$$

where $v_j,\ j = 1, 2, 3$ are the choosen expansion functions defined over the entire domain and $c_j, j = 1, 2, 3$ are constant coefficients to be determined. Substituting (3.6) into (3.5), we have (3.7)

$$F(\hat{\Phi}) = 0.5 \vec{c_j}^T \int_\Omega \vec{v} \mathscr{L} \vec{v}^T d\Omega \vec{c} - \vec{c}^T \int_\Omega \vec{v} f d\Omega \tag{3.7}$$

To minimize $F(\hat{\Phi})$, we force its partial derivatives with respect to c_j to vanish. This yields a set of linear algebraic equations as (3.8)

$$\begin{aligned} \frac{\partial F(\hat{\Phi})}{\partial c_j} &= 0.5 \int_\Omega \vec{v_i} \mathscr{L} \vec{v}^T d\Omega \vec{c} + 0.5 \vec{c}^T \int_\Omega \vec{v} \mathscr{L} v_i d\Omega - \int_\Omega v_i f d\Omega \\ &= 0.5 \sum_{j=1}^{N} c_j \int_\Omega (v_i \mathscr{L} v_j + v_j \mathscr{L} v_i) d\Omega - \int_\Omega v_i f d\Omega \\ &= 0 \qquad\qquad i = 1, 2, ..., N \end{aligned} \tag{3.8}$$

which can be written as the matrix equation (3.9)

$$[S]\vec{c} = \vec{b} \tag{3.9}$$

with the elements in matrix $[S]$ given by (3.10)

$$S_{ij} = 0.5 \int_{\Omega} v_i \mathscr{L} v_j d\Omega \tag{3.10}$$

An approximate solution for (3.1) is then given by (3.6) where c_j are obtained by solving the matrix (3.9).

Basic Steps of Ritz FEM

The Ritz FEM consists of a few basic steps as below

- Divide the domain into subdomains (elements) $\Omega_e,\ e = 1, 2, ..., M$
- Over each element, expand the unknown function as an interpolation of the values of the elements nodes $\phi^e = \sum_{j=1}^{N} N_j^e(\vec{r})\phi_j^e, r \in \Omega_e$, where ϕ_j^e is the value of ϕ at the j^{th} node of the e^{th} element and $N_j^e(\vec{r})$ is the corresponding interpolation function.
- Formulate the functional in terms of the unknown coefficients $F = \sum_{e=1}^{M} F^e(\hat{\phi}^e)$.
- Apply the opimality conditions for a minimize of the functional $\frac{\partial F}{\partial \phi_i} = 0, i = 1, 2, ..., N$
- Solve the resultant system of equations.

3.2.2 The Galerkin's Method

Galerkins method seeks a solution to the BVP in (3.1) by weighting the residual of the differential equation, so it is a member of the weighted residual methods. Assume that $\hat{\Phi}$ is an approximate solution to (3.1). Then the residual is

$$r = \mathscr{L}\hat{\Phi} - f \tag{3.11}$$

The best approximation for $\hat{\Phi}$ will be the one that resuces the residual to the least value at all points of Ω. We define the ith weighted residual as

$$R_i = \int_\Omega w_i r d\Omega = 0 \tag{3.12}$$

where are chosen weighting functions. When the weighting functions are selected as

$$w_i = v_i \qquad\qquad i = 1, 2, ..., N \tag{3.13}$$

It usually leads to the most accurate solution. So that (3.12) becomes

$$R_i = \int_\Omega (v_i \mathscr{L}\vec{v}^T\vec{c} + v_i f) d\Omega = 0 \qquad\qquad i = 1, 2, ..., N \tag{3.14}$$

This again will lead to (3.9). The FEM formula is the same between Ritz FEM and Galerkin's FEM now. The difference is only the selection of the trial function. In this thesis, the Ritz FEM is utilized. If interested, please refer to [3] for the Galerkin's method.

3.3 Finite Element Meshes

The finite element meshes can be classified into two types based on the nature of element: two-dimensional (2D) and there-dimensional (3D) meshes. Most popular 2D mesh are quadrilaterals and triangles as shown in Figure (3.2) and for 3D mesh, there are hexahedra, tetrahedra, square pyramids and extruded triangles shown in Figure (3.3). Each element is independent locally but is connected to each other globally but the field tangential continuous condition. In this thesis, the 3D waveguide mode problems are analyzed so only 2D meshes are used, specifically the triangles because good discretization could be achieved.

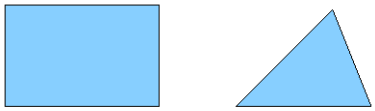

Figure 3.2: 2D finite element meshes

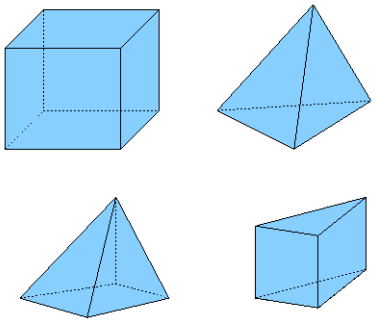

Figure 3.3: 2D finite element meshes

Chapter 4

Scalar FEM

4.1 Scalar Mode Equation

Scalar wave equation for 2D straight waveguide can be used to simulate the propagation of electromagnetic fields in optical waveguides with relative weak refractive index difference over the cross section. The scalar wave equation (2.15) for an inhomogeneous isotropic medium is rewritten as

$$\nabla_t^2 \phi + k^2 \phi = 0 \tag{4.1}$$

where k^2 is the eigenvalue. With (3.7), we could derive the corresponding functional given by (4.2) as

$$F(\phi) = 0.5 \iint_\Omega [(\frac{\partial \phi}{\partial x})^2 + (\frac{\partial \phi}{\partial y})^2 - k^2 \phi^2] ds \tag{4.2}$$

where Ω represents the cross-sectional area of the waveguide. And

$$k^2 = n^2 k_0^2 - \beta^2 \tag{4.3}$$

where $k_0 = \frac{2\pi}{\lambda_0}$ is the free space wave number, n the refractive index of the medium, which varies across the cross-sectional area, and β the propagation constant.

4.2 Finite Element Formula

4.2.1 FEM Approximation

For numerical simulation, the cross-sectional area is discretized into small triangles, called elements. Hence we discretized functional (4.2) and get (4.4)

$$F(\phi) = \sum_{e=1}^{N_e} \iint_{\Omega} 0.5[(\frac{\partial \phi_e}{\partial x})^2 + (\frac{\partial \phi_e}{\partial y})^2 - k^2 \phi_e^2] ds \tag{4.4}$$

where e represents the element number, N_e represents the total number of elements and Ae represents the area of the element e over which the functions are integrated.

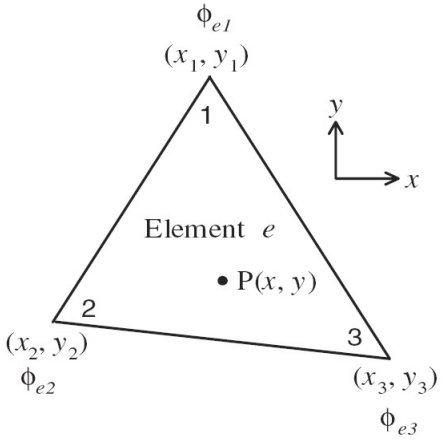

Figure 4.1: First order triangular element

As shown in Figure (4.1), the ϕ value at the point of $P(x, y)$ inside the triangle

may be approximated linearly as (4.5)

$$\phi(x,y) = a + bx + cy \tag{4.5}$$

$$\phi(x,y) = [N(x,y)]^T\{\phi_e\} \tag{4.6}$$

where

$$\{\phi_e\} = [\phi_{e1}\ \phi_{e2}\ \phi_{e3}]^T$$

and

$$N = [N(x,y)] = \begin{bmatrix} L_1 \\ L_2 \\ L_3 \end{bmatrix} = \frac{1}{2A_e}\begin{bmatrix} a_1 & b_1 & c_1 \\ a_2 & b_2 & c_2 \\ a_3 & b_3 & c_3 \end{bmatrix}\begin{bmatrix} 1 \\ x \\ y \end{bmatrix} \tag{4.7}$$

with

$$2A_e = \det\begin{bmatrix} 1 & 1 & 1 \\ x_1 & x_2 & x_3 \\ y_1 & y_2 & y_3 \end{bmatrix} \tag{4.8}$$

$$a_k = x_l y_m - x_m y_l \quad b_k = y_l - y_m \quad c_k = x_m - x_l \tag{4.9}$$

where x_k, y_k $(k = 1, 2, 3)$ are the Cartesian coordinates of the corner points 1 to 3 of the triangle and the subscripts k, l, m are 1,2,3; 3,1,2; 2,3,1, which are cyclically progressing around the threee vertices of the triangle. Hence we have (4.10) and (4.11)

$$\frac{\partial\phi_e(x,y)}{\partial x} = \{\mathbf{b}\}\{\mathbf{\Phi_e}\} \tag{4.10}$$

$$\frac{\partial\phi_e(x,y)}{\partial y} = \{\mathbf{c}\}\{\mathbf{\Phi_e}\} \tag{4.11}$$

which are not dependent on x and y, with $\{\mathbf{b}\} = [b_1, b_2, b_3], \{\mathbf{c}\} = [c_1, c_2, c_3]$ and $\{\mathbf{u}\} = [a_1 + b_1x + c_1y, a_2 + b_2x + c_2y, a_3 + b_3x + c_3y]$, functional (4.4) could be written as (4.12)

$$\begin{aligned} F(\phi) &= 0.5 \iint_{\Omega} [(\frac{\partial \phi}{\partial x})^2 + (\frac{\partial \phi}{\partial y})^2 - k^2\phi^2] d\Omega \\ &= 0.5 \sum_{e=1}^{N_e} \iint_{\Omega} [(\{\mathbf{b}\}\{\mathbf{\Phi_e}\})^T \{\mathbf{b}\}\{\mathbf{\Phi_e}\} + (\{\mathbf{c}\}\{\mathbf{\Phi_e}\})^T \{\mathbf{c}\}\{\mathbf{\Phi_e}\} \\ &\quad - k^2(\{\mathbf{u}\}\{\mathbf{\Phi_e}\})^T \{\mathbf{u}\}\{\mathbf{\Phi_e}\}] d\Omega \\ &= 0.5 \sum_{e=1}^{N_e} [\{\mathbf{\Phi_e}\}^T [\mathbf{P_e}] \{\mathbf{\Phi_e}\} - k^2 \{\mathbf{\Phi_e}\}^T [\mathbf{Q_e}] \{\mathbf{\Phi_e}\}] \end{aligned} \tag{4.12}$$

where

$$[\mathbf{P_e}] = A_e[\{\mathbf{b}\}^T\{\mathbf{b}\} + \{\mathbf{c}\}^T\{\mathbf{c}\}] \tag{4.13}$$

and

$$[\mathbf{Q_e}] = \frac{A_e}{12} \begin{pmatrix} 2 & 1 & 1 \\ 1 & 2 & 1 \\ 1 & 1 & 2 \end{pmatrix} \tag{4.14}$$

with the help of

$$\iint_{\Omega} u_1^l u_2^m u_3^n d\Omega = A_e \frac{l!m!n!2!}{(l+m+n+2)!} \tag{4.15}$$

to abtain $[\mathbf{Q_e}]$.

4.2.2 FEM Matrix

Please note that, in (4.2.1), the subscripts of e in $[\mathbf{P_e}]$ and $[\mathbf{Q_e}]$ means these 3 by 3 matrixes are local matrixes. But the operation of summation $\sum_{e=1}^{N_e}$ means the assembling process, a mapping process in reality, of the local matrixes to global matrixes of $[\mathbf{P_g}]$ and $[\mathbf{Q_g}]$, which are N_n by N_n matrixes, where N_n is the number of nodes.

Thus, functional (4.12) can be written as (4.16)

$$F(\phi) = 0.5[\{\mathbf{\Phi_e}\}^T[\mathbf{P_g}]\{\mathbf{\Phi_e}\} - k^2\{\mathbf{\Phi_e}\}^T[\mathbf{Q_g}]\{\mathbf{\Phi_e}\}] \tag{4.16}$$

where $[\mathbf{P_g}] = \sum_{e=1}^{N_e}[\mathbf{P_e}]$ and $[\mathbf{P_g}] = \sum_{e=1}^{N_e}[\mathbf{P_e}]$

4.2.3 Forming FEM Equations

The finite element solution is obtained by minimising the functional (4.16) with respect to each of the nodal values. Set

$$\frac{\partial F(\phi)}{\partial \phi_k} = 0 \quad \text{for} \quad k = 1, 2, ..., N_n \tag{4.17}$$

Thus we have

$$\{\mathbf{P_g}\}[\mathbf{\Phi}] - k^2\{\mathbf{Q_g}\}[\mathbf{\Phi}] = \mathbf{0} \tag{4.18}$$

4.3 PML Scheme in Finite Element Method

For many years, PML is most implemented as numerical boundary condition in many mode solvers with Finite Different in Time Domain (FDTD) or Finite Different Method (FDM), such as those in [4] and [5]. In this thesis, we are going to

apply the PML in the technique of Finite Element Method in frequency domain.

According to the modified Maxwell equations, PML can be seen as anisotropic medium with complex refractive index contribution within the layer. However, as in section 2.2, we can used the coordinate stretching method [5] to solve the equations.

4.3.1 The complex coordinate-stretching factor

The complex coordinate is

$$\tilde{p} = \int_0^p \alpha_p(p')dp' \tag{4.19}$$

where $p = x, y$, we got

$$\frac{1}{\alpha_p}\frac{d}{dp} = \frac{d}{d\tilde{p}} \tag{4.20}$$

and

$$\tilde{d}_{PMLp} = \int_{p_0}^{p_1} \alpha_p(p')dp' \tag{4.21}$$

Thus PML medium is regarded as a real medium with complex spatial coordinates or thickness.

For $\sigma_p(\rho)$,where $\rho = x - x_0$, the reflection coefficient is

$$R_{PMLp}(\phi) = \exp\{-\frac{2cos\phi}{n_{PML}\sqrt{\epsilon_0/\mu_0}}\int_0^{d_{PML}} \sigma_p(\rho)d\rho\} \tag{4.22}$$

where ρ is the distance to the interface inwards between PML and inner medium and ϕ is the incident angle to the normal of the interface. We can see that the best performance occurs while the incident wave is perpendicular to the interface.

The conductivity $\sigma_p, p = x, y$ is gradually growing from zero to the maximum value σ_{max}. There are various profiles for the conductivity specified by a profile function

$f_p(\rho)$ as below

$$\sigma_p = f_p(p) \cdot \sigma_{max} \tag{4.23}$$

For polynomial grading of the conductivity used in this thesis, we set

$$f_p(\rho) = (\frac{\rho}{d_{PMLp}})^m \tag{4.24}$$

Typically optimal values are $2 \leq n \leq 6$. And the bigger m is, the smoother the change of $\sigma_p(p)$ close to the interface and the steeper to the PRB boundary,which means reflection occurs deeper numerically in the PML region close to the PRB.

With Equation (4.22), the reflection coefficient is as below [4]

$$R_{PMLp}(\phi) = \exp\{-\frac{2\sigma_{max}cos\phi}{n_{PML}\sqrt{\epsilon_0/\mu_0}}\int_0^{d_{PML}}(\frac{\rho}{d_{PMLp}})^m d\rho\} \tag{4.25}$$

And we solve σ_{max} and plug into the complex coordinate-stretching factor in (2.23), we have

$$\alpha(\phi,\rho)_p = 1 - j\frac{\lambda}{4\pi n_{PMLp}d_{PMLp}cos\phi}[(m+1)ln(\frac{1}{R_{PMLp}})](\frac{\rho}{d_{PMLp}})^m \tag{4.26}$$

As we could see from Equation (4.26), unlike the 1-D problems, the complex coordinate-stretching factor is α and the incident angle ϕ dependent if we set a R_{PMLp}. However, in most of the pratical problems, PML is placed relatively far from the core region, thus ϕ is arround 0. Let's set $\phi \approx 0$, we have (4.27). Please note that in corner region, the reflection is larger.

$$\alpha(\rho)_p = 1 - j\frac{\lambda}{4\pi n_{PMLp}d_{PMLp}}[(m+1)ln(\frac{1}{R_{PMLp}})](\frac{\rho}{d_{PMLp}})^m \tag{4.27}$$

4.3.2 PML Scheme in 2-D Problems

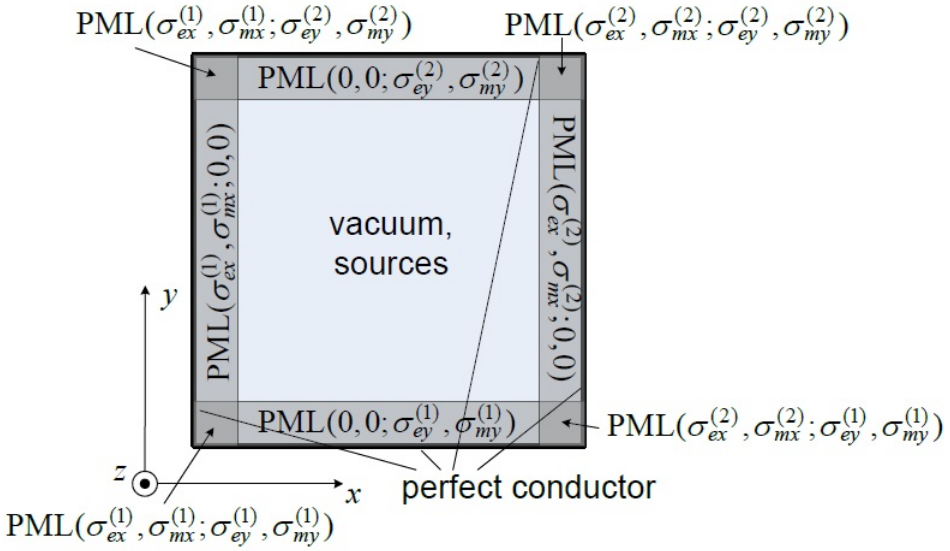

Figure 4.2: PML + PRB Scheme in 3-D Waveguides

The PML scheme in 3D waveguide cross section used in this thesis is shown in Figure (4.17). If the interface of PML inwards is perpendicular to x(or y) direction, the waves attenuate along x(or y) direction and the conductivity of y(or x) direction must be zero in order to ensure the tangential continuity. At the corner region, either is zero. And the complex coordinate-stretching factor in (4.27) is applied.

If the waveguide extends to the PML region shown in Figure (4.3), as in Ridge waveguides where in theory it is boundless along x direction, we could set the refractive index in the PML region A, B,C values of n_1, n_0, n_0 naturally.

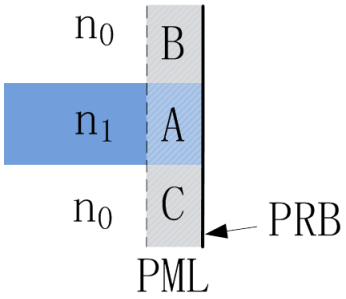

Figure 4.3: Overlap section between waveguide and PML

4.4 Validation of Scalar FEM with PRB Boundary Condition

Numerical examples with Scalar FEM for circular waveguide (two-layer step-index optical fiber particularly in this thesis), rectangular dieletric waveguide and ridge waveguide are presented in this section, which are all typical examples and structures widely used in the opitical area.

4.4.1 Circular Waveguide

Analytical Modal analysis of Step-index Fiber

In [7] chapter 3, a rigorous analysis of step-index fiber as in Figure (4.4), including TE, TM and Hybrid Modes, is presented as well as the Linearly Polarized (LP) modes, which are important in practical weakly guiding fibers. For more details, please refer to chapter 3 in [7] . The dispersion relationships are concluded as in Table (4.1).

In most of the circumstances, the refractive-index difference Δ of practical fiber is of the order of 1%. Thus, with the approximation of $n_1/n_0 \approx 1$, the analysis of

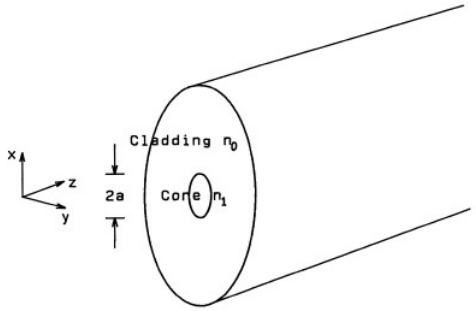

Figure 4.4: Circular waveguide

optical fiber could be simplified as Table (4.2).

The approximation of $n_1/n_0 \approx 1$ means the confinement in the core is not so tight. Thus it is called weakly guiding approximation. And this group of modes under the approximation is designed as Linearly Polarized(LP) modes. Compare the relation between LP modes in Table (4.2) and conventional rigorous mode in Table (4.1), we could conclude the LP modes as in Table (4.3).

Numerical Results of Circular Waveguide Example

Modal analysis of two-layer step-index fiber as in Figure (4.4) with Scalar FEM is presented in this section. Simulation is implemented of cross-section as in Figure (4.5) with PRB condition applied. The parameters are listed in Table (4.4).

The fundamental mode profile is shown in Figure (4.7).Figure (4.6) is an example of the finite element mesh grids. The effective refractive index of the fundamental mode compared to the analytical effective refractive solved with the previous discussed dispersion equations is shown in Table (4.5). Figure (4.8) shows the convergence of the fundamental mode.

Table 4.1: Dispersion equations for conventional rigorous modes in the step-index ciruclar waveguide

Mode Designation ($l \geq 1$)	**Dispersion equation**
TE_{0l}	$\frac{J_1(u)}{uJ_0(u)} = -\frac{K_1(w)}{wK_0(w)}$
TM_{0l}	$\frac{J_1(u)}{uJ_0(u)} = -(\frac{n_0}{n_1})^2\frac{K_1(w)}{wK_0(w)}$
Hybrid($n \geq 1$)	$[\frac{J_n'(u)}{uJ_n(u)} + \frac{K_n'(w)}{wK_n(w)}][\frac{J_n'(u)}{uJ_n(u)} + (\frac{n_0}{n_1})^2\frac{K_n'(w)}{wK_n(w)}]$ $= n^2(\frac{1}{u^2} + \frac{1}{w^2})[\frac{1}{u^2} + \frac{n_0}{n_1})^2\frac{1}{w^2}]$

Note: $J_n(u)$ is the n-th order Bessel function and $K_n(w)$ the 0-th order Bessel function of second kind. u and w is the transverse wave numbers with $u = \kappa a = a\sqrt{k_0^2 n_1^2 - \beta^2}$ and $w = \sigma a = a\sqrt{\beta^2 - k_0^2 n_0^2}$. Normalized frequency v is given as $v^2 = u^2 + w^2 = k_0^2(n_1^2 - n_0^2)$. l means the $l-th$ zero-point of the dispersion equation.

Table 4.2: Dispersion equations under the weakly guiding approximation

Mode Designation ($l \geq 1$)	**Dispersion equation**
TE_{0l} or TM_{0l}	$\frac{J_1(u)}{uJ_0(u)} = -\frac{K_1(w)}{wK_0(w)}$
$EH_{nl}, n \geq 1$	$\frac{J_{n+1}(u)}{uJ_n(u)} = \frac{K_{n+1}(w)}{wK_n(w)}$
HE_{1l}	$\frac{J_0(u)}{uJ_1(u)} = \frac{K_0(w)}{wK_1(w)}$
$HE_{nl}, n \geq 2$	$\frac{J_{n-1}(u)}{uJ_{n-2}(u)} = -\frac{K_{n-1}(w)}{wK_{n-2}(w)}$

Note: Same with Table (4.1).

Table 4.3: Comparison of dispersion equations between LP and conventional modes

LP Mode ($l \geq 1$)	**Conventional Mode**	**Dispersion equation**
LP_{0l}	HE_{1l}	$\frac{J_0(u)}{uJ_1(u)} = \frac{K_0(w)}{wK_1(w)}$
LP_{1l}	TE_{0l} TM_{0l} HE_{2l}	$\frac{J_1(u)}{uJ_0(u)} = -\frac{K_1(w)}{wK_0(w)}$
$LP_{ml}, m \geq 2$	$HE_{m+1,l}$ $EH_{m-1,l}$	$\frac{J_m(u)}{uJ_{m-1}(u)} = -\frac{K_m(w)}{wK_{m-1}(w)}$

Note: Same with Table (4.1).

Table 4.4: Parameters of the step-index circular waveguide shown in Figure (4.5)

Parameter	**Value**	**Unit**
r	0.6	μm
n_1	2.36	
n_2	2.2	
lambda	1.55	μm

Note: Box size is length×width = $2.4\mu m$*$2.4\mu m$, enclosed by PRB.

Table 4.5: Effective refractive index for LP modes

	Scalar FEM		
Mode Type	**1038 nodes**	**1894 nodes**	**Analytical Values**
LP_{01}	2.271154	2.271437	2.271900

Note: Single mode fiber condition: normalized frequency $v = \frac{2\pi a}{\lambda}\sqrt{n_1^2 - n_2^2} < 2.405$

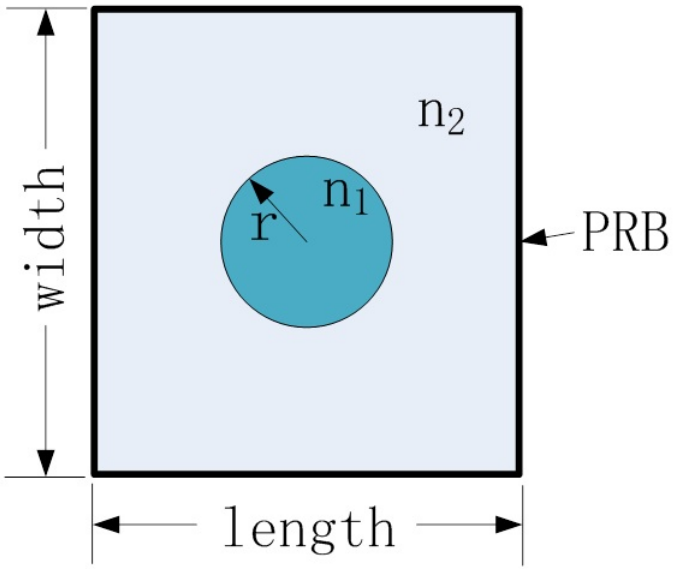

Figure 4.5: Cross section of a circular waveguide with PRB

4.4.2 Rectangular Dielectric Waveguide

Another examples, a rectangular dielectric waveguide (known as buried waveguide) is also presented. The buried waveguide cross section are shown as Figure (4.9), and its parameters are shown in Table (4.6). The finite element meshes are shown as Figure (4.10). The simulation results are shown in Table (4.7). E field mode profiles are as Figure (4.11)

4.4.3 Ridge Waveguide

The modes of a typical integrated optical waveguide such as the one shown in Figure (4.12) can be separated into two groups: the E^x_{pq} modes (also called H^y_{pq} modes or HE_y modes) and the E^y_{pq} modes (also called H^x_{pq} modes or EH_y modes), where p and q are the mode numbers. And further more, these two kinds of mode could be

Table 4.6: Parameters of the buried waveguide

Parameter	**Value**	**Unit and Note**
w_{wg}	0.8	μm
l_{wg}	0.8	μm
n_1	3.54	Core
n_2	3.17	Cladding
λ_0	1.30	μm

Note: Box size is length×width = $2.4\mu m$*$2.4\mu m$, enclosed by PRB.

Table 4.7: Effective refractive index of the buried waveguide

	Simulation n_{eff}, Node Number	
Mode Type	**800**	**2172**
1st	3.434063	3.434041
2nd	3.282078	3.281872
3rd	3.282067	3.282036

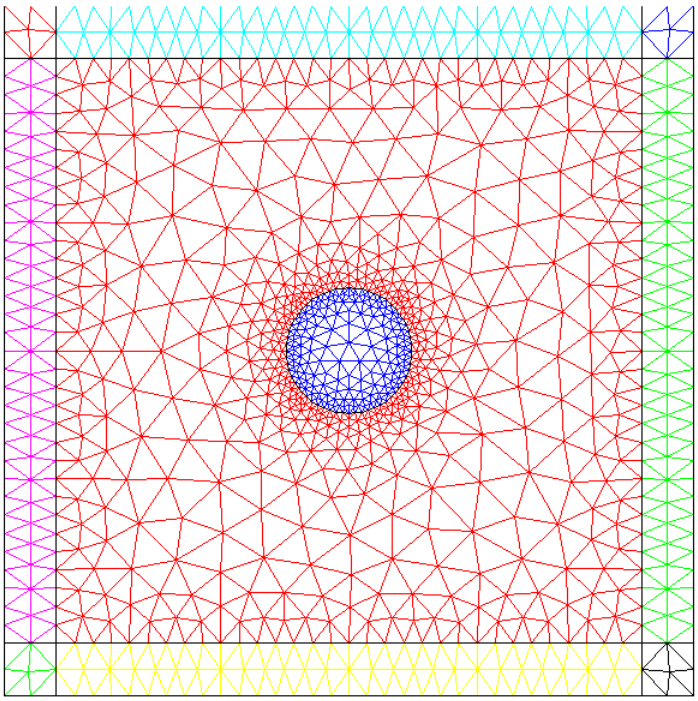

Figure 4.6: Finite element meshes of the step-index fiber

approximated by the TE_y ($E_y = 0$) and TM_y ($M_y = 0$), respectively. And If the refractive index along the x-direction varies slowly in the area where the energy is concentrated, these TE_y and TM_y modes can in turn be approximated by quasi-TE modes and quasi-TM modes for which E_z and H_z are negligibly small, respectively.

Numerical Results of Ridge Waveguide Example

Modal analysis of a ridge waveguide as in Figure (4.12) with Scalar FEM is presented in this section. Simulation is implemented of cross-section as in Figure (4.13) with PRB condition applied. The parameters are listed in Table (4.8). The finite element meshes are shown in Figure (4.14).

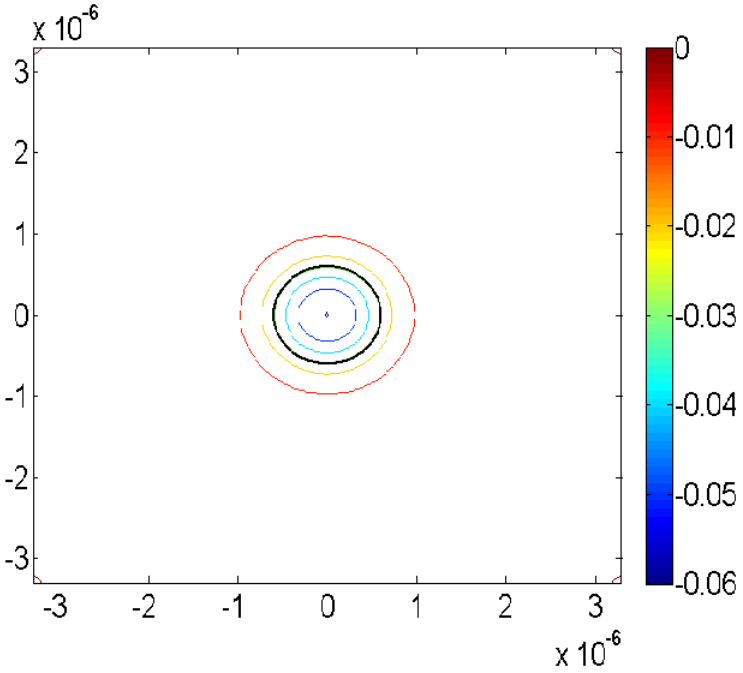

Figure 4.7: Fundamental mode amplitude. Note that phase of the profile is -π

The guided mode profiles are shown in Figure (4.15). And the effective refractive index compared to the papers in [2] is shown in Table (4.9).

4.5 Validation of Scalar FEM with PML and PRB Boundary Condition

4.5.1 Examples

Applying PML to the boundary of the examples the of circular waveguide and ridge waveguide in Chapter 4, we have the structure as Figure (4.17) and Figure(4.19). And the results are shown in Table (4.10) and Table (4.11) below. The convergence

Table 4.8: Parameters of the ridge waveguide in Figure (4.12)

Parameter	**Value**	**Unit**
w	2.4	μm
t	0.0,0.2,0.4	μm
h	1.0,0.8,0.6	μm
d	0.2	μm
n_c	3.38	
n_s	3.17	
n_a	1.0	
λ_0	1.55	μm

Note: Box size is length×width = $3.0\mu m$*$3.6\mu m$, enclosed by PRB.

Table 4.9: Effective Refractive index for the fundamental quasi-TE mode

	Scalar FEM		Reference Values[2]	
Mode Type	**1200 nodes**	**2000 nodes**	**SFEM**	**VFEM**
t = 0.0 μm	3.1949595,1333	3.1950611,1929	3.1965312	3.1945511
t = 0.2 μm	3.1990136,1254	3.1992126,2019	3.1995419	3.1983379
t = 0.4 μm	3.2029277,1314	3.2030688,1994	3.2024854	3.2021418

Note: For purpose of comparison of published results in [2], with normalized frequency $b = \dfrac{n_{eff}^2 - n_s^2}{n_c^2 - n_s^2}$, we convert b in the paper to the n_{eff} shown in the table. Please note that for quasi-TE ($\partial\phi/\partial n = 0$) and quasi-TM ($\phi = 0$).

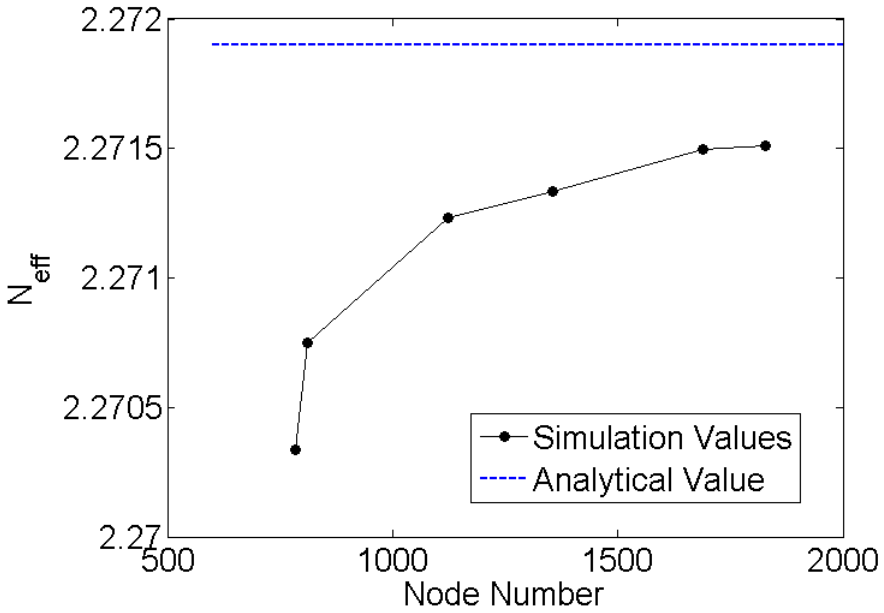

Figure 4.8: Convergence of effective index of the fundamental mode

of the imaginary part of n_{eff} is shown in Figure (4.18)

Figure (4.16) is the 3rd mode of ridge waveguide where we can see the difference before and after applying PML BC.

4.5.2 Orthogonality

In many application of modes, for example the Mode Matching Method, the basic preposition is always the completeness and orthogonality within modes, which makes it important to validate the orthogonality between modes.

In General, the time average power for the m-th mode is [8]

$$\frac{1}{4}\iint_{\Omega}(\vec{E}_{tn}\times\vec{H}^{*}_{tn}+\vec{E}^{*}_{tn}\times\vec{H}_{tn})\cdot\hat{z}ds=P_{n} \tag{4.28}$$

Table 4.10: Effective Refractive index of LP modes of step-index circular waveguide

	Scalar FEM 1955 nodes		
Mode Type	**PML+PRB**	**PRB**	**Analytical Values**
LP_{01}	2.2714369+8.26e-9i	2.2714368	2.271900
2nd	2.1896205+7.28e-5i	2.1886926	

Note: $R_{PML} = 10^{-3}$, $d_{PML} = 0.4 \times 10^{-6}$

Table 4.11: Effective refractive index of the buried waveguide

	Simulated n_{eff}, 2172 nodes	
Mode Type	**PML+PRB**	**PRB**
1st	3.434559+1.21e-7i	3.434041
2nd	3.283670+5.84e-6i	3.281872
3rd	3.283659+5.82e-6i	3.282036

Note: $R_{pml} = 10^{-3}$

Table 4.12: Effective refractive index for the fundamental quasi-TE mode in the ridge waveguide

	SFEM 2000 nodes		Reference Values[2]
Mode Type	**PRB+PML**	**PRB**	**SFEM**
t = 0.0 μm	3.1949708+7.69e-5i	3.1950611	3.1965312
t = 0.2 μm	3.1983795+4.38e-4	3.1992126	3.1995419
t = 0.4 μm	3.2003960+4.62e-4i	3.2030688	3.2024854

Note: $R_{pml} = 10^{-4}$. Others is the same with Table (**??**).

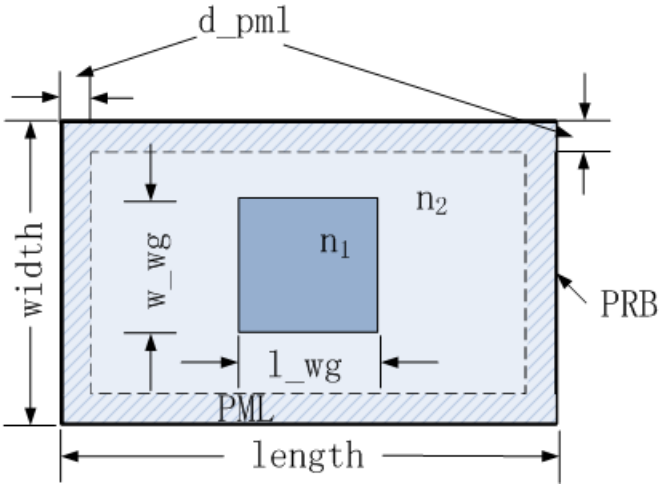

Figure 4.9: Cross section of a buried waveguide

where Ω is the entire region, asterisk denotes complex conjugate and power carried by each mode is normalized to 1 by the power P_n.

We could derive the mode orthogonality between n-th and m-th mode from Reciprocal Theorem as (4.29)

$$< \vec{E}_{tn}, \vec{H}_{tm} >= \frac{1}{4} \iint_{\Omega} (\vec{E}_{tn} \times \vec{H}_{tm} + \vec{E}_{tn} \times \vec{H}_{tm}) \cdot \hat{z} ds = \delta_{mn} \tag{4.29}$$

which is denoted as General Orthogonality property which holds for media with loss or gain.

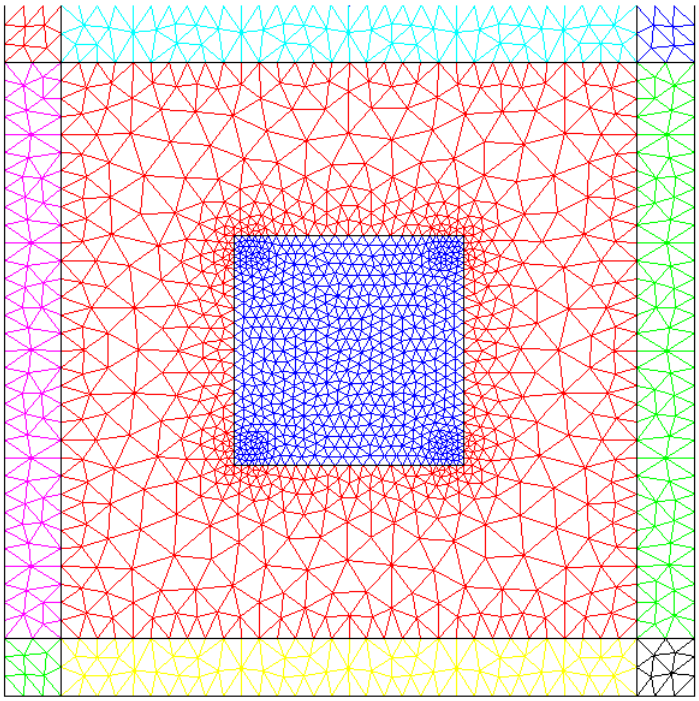

Figure 4.10: Cross section of a buried waveguide

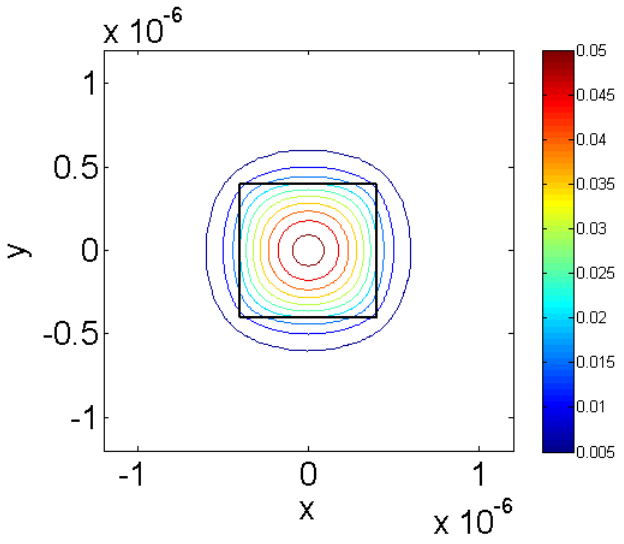

(a) 1st mode

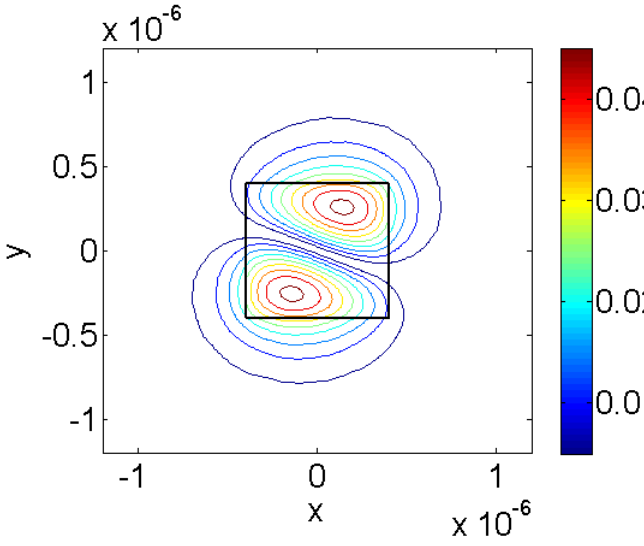

(b) 2nd mode

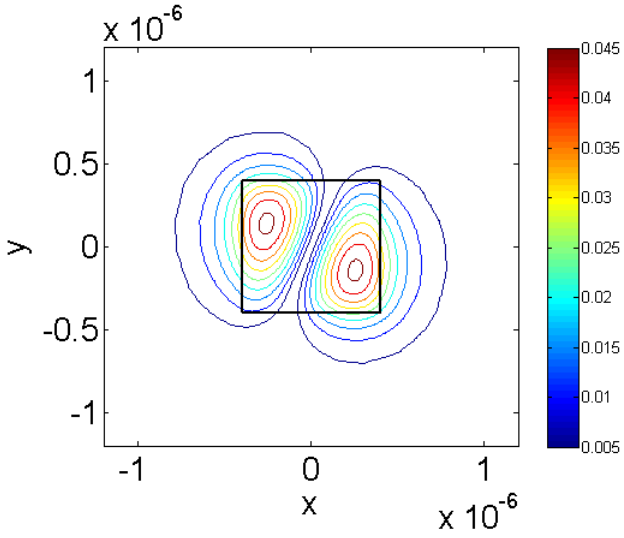

(c) 3rd mode

Figure 4.11: Guided mode amplitude of rectangular dielectric waveguide. Note that phase of the profiles are -π in fundamental mode and either π or -π in 2nd and 3rd modes

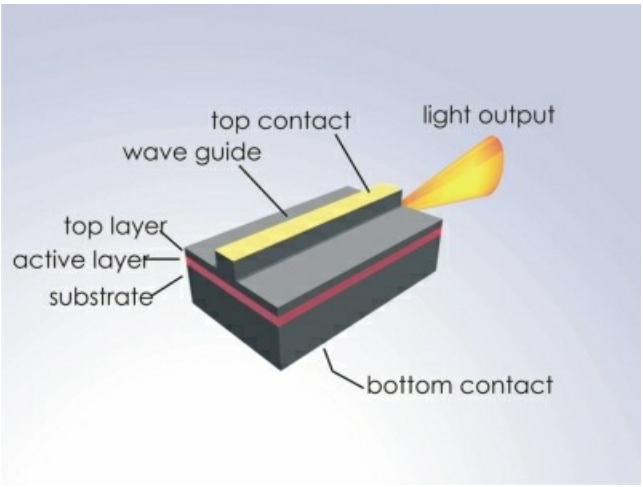

Figure 4.12: Ridge waveguide

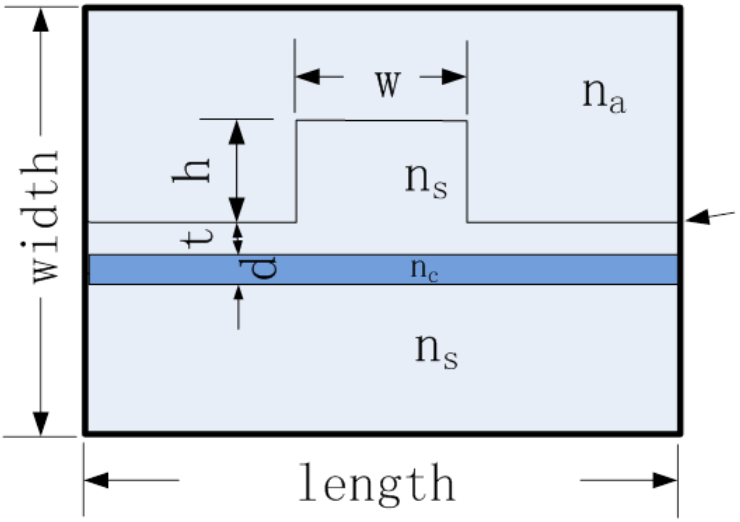

Figure 4.13: Cross section of a ridge waveguide with PRB

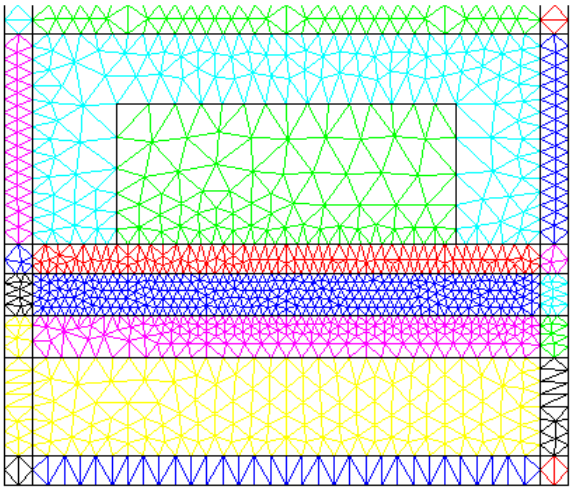

Figure 4.14: Cross section of a ridge waveguide with PRB

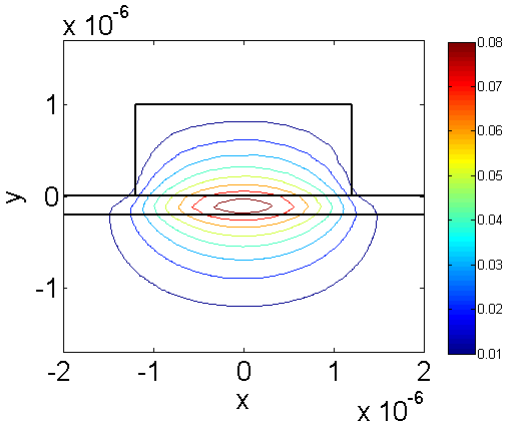

(a) t=0.0 μm

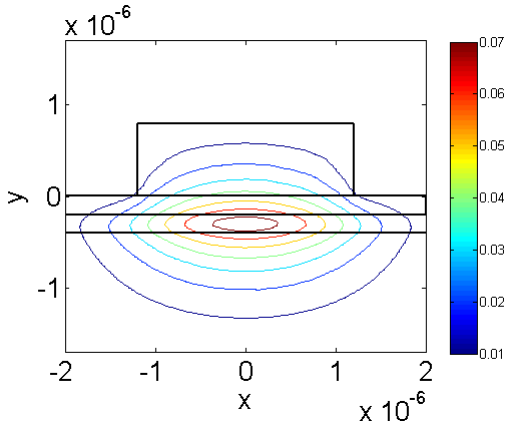

(b) t=0.2 μm

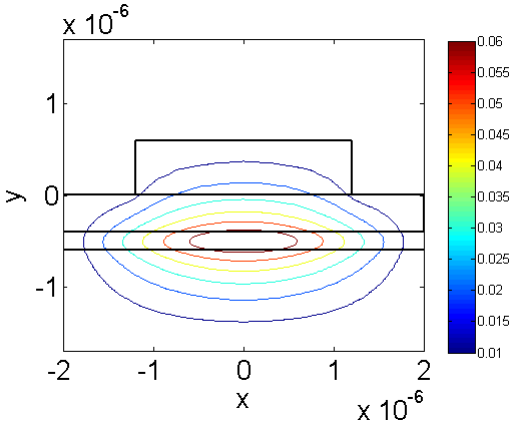

(c) t=0.4 μm

Figure 4.15: Guided mode amplitude of ridge waveguide. Note that phase of the profile is the same, π

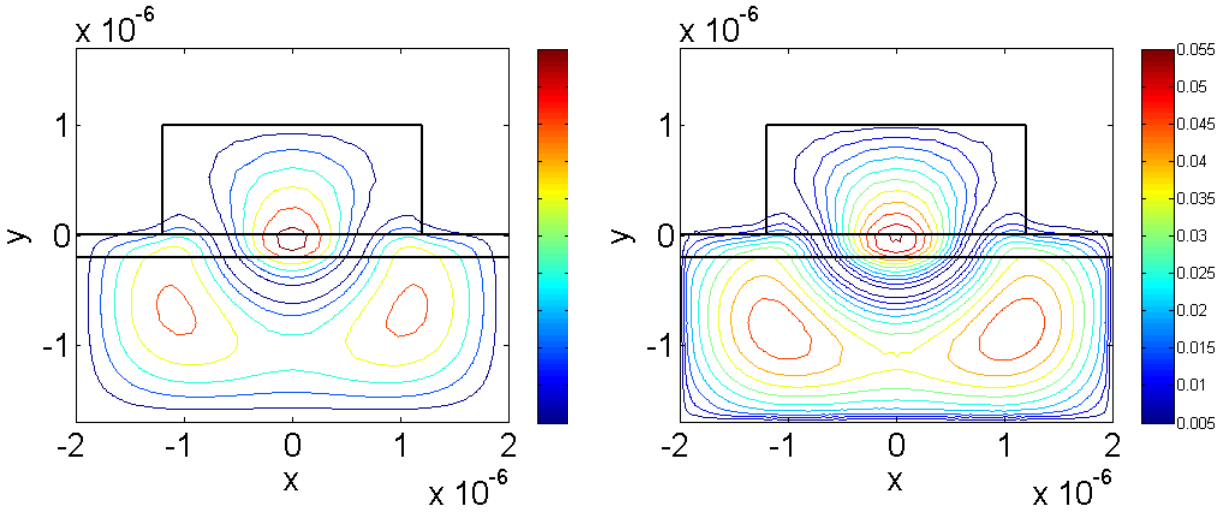

(a) 1st mode (b) 2nd mode

Figure 4.16: 3rd mode amplitude of ridge waveguide (t=0). Note that phase of the profiles is either π or -π

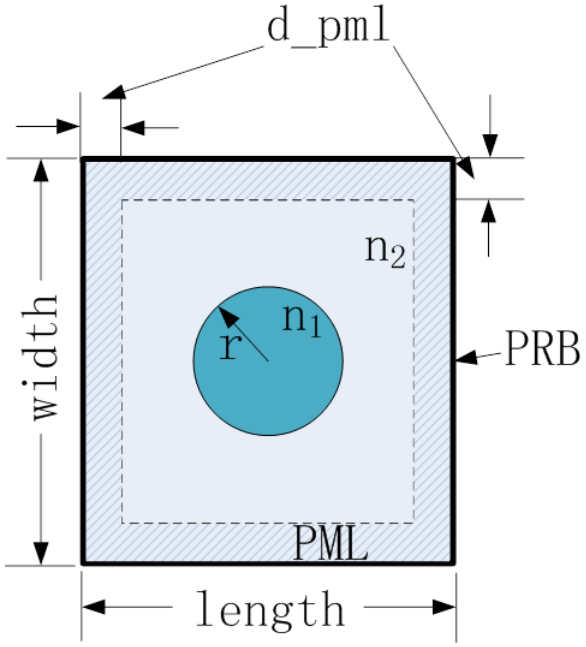

Figure 4.17: Cross section of a circular waveguide with PML + PRB

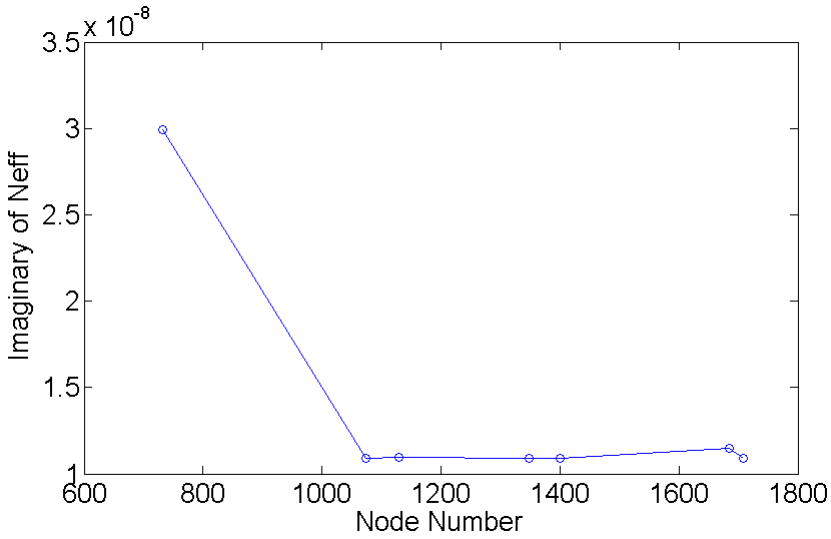

Figure 4.18: Convergence of the imaginary part of effective refractive index of the fundamental mode for step-index circular waveguide

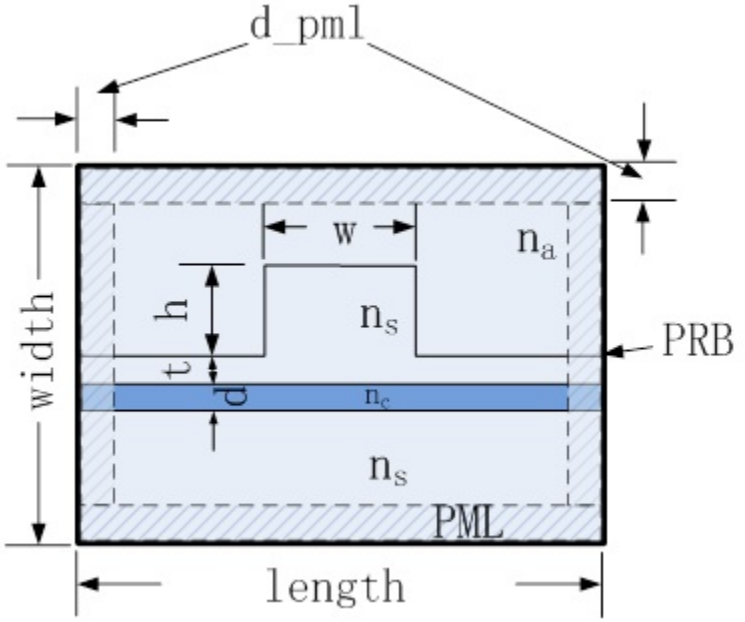

Figure 4.19: Cross section of a ridge waveguide with PML + PRB

Chapter 5

Vectorial FEM

For strong guided problems, the scalar FEM is not that accurate. Thus, the vectorial FEM is derived in this chapter. However, nodal-based FEM as shown in Figure (4.1) is proved that nonphysical or spurious solutions, which are generally attributed to the lack of enforcement of divergence condition [9], appear. So we introduce edge-based FEM [10] [11] [12]. There are various types of edge-based meshes [10]. We will use one as Figure (5.1) shows.

5.1 Nodal, edge-based Vectorial FEM and Spurious Modes

The full vector equation (2.11) and (2.12) are often discretized by the nodal vectorial elements, which is vector-valued, continuous, piecewise linear basis fields, and thus determined by degrees of freedom which are the nodal values of the field. However, there are two drawbacks of this approach: the difficulty to set boundary conditions

and the failure to converge. The former, a minor drawback, means that a normal has to be defined at boundary nodes but there is no rational basis for such definition. The latter is a major drawback witch the essential argument on which to base a converge proof is lacking, thus the convergence cannot be guaranteed [9]. Thus the nodal vectorial FEM is a non-consistent method.

A new edge-based vectorial FEM, which is consistent, became popular in the 90's. It gives the right kind of continuity for H field and E field on the boundary. And more important, edge-based elements are consistent. The convergence of this numerical scheme is proposed in [9].

Also in [9], the question of spurious mode is raised. Spurious modes are the wrong, divergent modes which could be solved together with the convergent modes by conventional modes, such as nodal vectorial FEM. It is obviously not acceptable as physical solutions. But yet it have "polluted" the mode spectrum for years. However, the tangential continuous edge-based FEM in this thesis would solve the problem.

5.2 Edge-based Finite Element Formula

5.2.1 Full Vectorial Mode Equation

The Functional for (2.7) is given by (5.1)

$$F = \iint_{\Omega} [(\nabla \times \mathbf{\Phi})^* \cdot ([p]\nabla \times \mathbf{\Phi}) - k_0^2[q]\mathbf{\Phi}^* \cdot \mathbf{\Phi}]dxdy \tag{5.1}$$

where Ω is the waveguide cross section [11]. Consider anisotropic medium of (5.2)

$$[p] = \begin{pmatrix} p_x & 0 & 0 \\ 0 & p_y & 0 \\ 0 & 0 & p_z \end{pmatrix} \quad [q] = \begin{pmatrix} q_x & 0 & 0 \\ 0 & q_y & 0 \\ 0 & 0 & q_z \end{pmatrix} \tag{5.2}$$

where

$$\begin{aligned} p_x &= p_y = p_z = 1, \\ q_x &= \epsilon_{rx} = n_x^2 \\ q_y &= \epsilon_{ry} = n_y^2 \\ q_z &= \epsilon_{rz} = n_z^2 \end{aligned} \tag{5.3}$$

for $\mathbf{\Phi} = \mathbf{E}$, and

$$\begin{aligned} p_x &= 1/\epsilon_{rx} = 1/n_x^2 \\ p_y &= 1/\epsilon_{ry} = 1/n_y^2 \\ p_z &= 1/\epsilon_{rz} = 1/n_z^2, \\ q_x &= q_y = q_z = 1 \end{aligned} \tag{5.4}$$

for $\mathbf{\Phi} = \mathbf{H}$.

5.2.2 Discretization

Nodal methods will cause the appearance of spurious solutions. For full vector finite scheme that we will use in this paper [11], three components on three edges of the triangles will get involved shown as Figure (5.1).

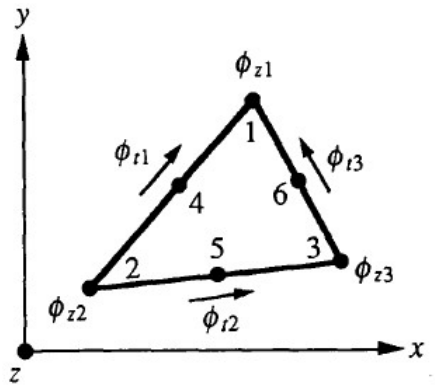

Figure 5.1: Edge triangular element

There are six nodes in this scheme which consist of three corner and three edge nodes. The corner nodes are for the axial components of the propagation direction ϕ_z, i.e. z direction, and the edge nodes are for the tangential components.

5.2.3 Shape functions

$\{\phi_z\}_e$ is the nodal axial-field vector for each element and $\{N\}$ is the ordinary shape function vector for each triangular element linearly.

$$\phi_z = jN(x,y)^T\{\phi_z\}_e = jN^T\{\phi_z\}_e \tag{5.5}$$

where $N = N(x,y)$ is the ordinary shape function for nodal element as shown in Chapter 4 equation (4.7).

ϕ_t is the tangential component of the triangle, i.e. $\phi_t = \mathbf{\Phi} \cdot \mathbf{t}$. The shape function for edge element are $U(y)$ and $V(x)$ as

$$\phi_x = U(y)^T \phi_{te} = U^T \phi_{te} \tag{5.6}$$

$$\phi_y = V(x)^T \phi_{te} = V^T \phi_{te} \tag{5.7}$$

where

$$U = \begin{pmatrix} \tilde{a}_1 + \tilde{c}_1 y \\ \tilde{a}_2 + \tilde{c}_2 y \\ \tilde{a}_3 + \tilde{c}_3 y \end{pmatrix} \tag{5.8}$$

$$V = \begin{pmatrix} \tilde{b}_1 - \tilde{c}_1 x \\ \tilde{b}_2 - \tilde{c}_2 x \\ \tilde{b}_3 - \tilde{c}_3 x \end{pmatrix} \tag{5.9}$$

with

$$\begin{aligned} \tilde{a}_k &= [(y_{m+3} cos\theta_{m+3} - x_{m+3} sin\theta_{m+3}) sin\theta_{l+3} - (y_{l+3} cos\theta_{l+3} - x_{l+3} sin\theta_{l+3}) sin\theta_{m+3}]/\Delta \\ \tilde{b}_k &= [(y_{l+3} cos\theta_{l+3} - x_{l+3} sin\theta_{l+3}) cos\theta_{m+3} - (y_{m+3} cos\theta_{m+3} - x_{m+3} sin\theta_{m+3}) cos\theta_{l+3}]/\Delta \\ \tilde{c}_k &= (cos\theta_{l+3} sin\theta_{m+3}) - cos\theta_{m+3} - sin\theta_{l+3})]/\Delta \end{aligned} \tag{5.10}$$

with

$$\Delta = \sum_{k=1}^{3} (y_{k+3} cos\theta_{l+3} - x_{k+3} sin\theta_{k+3}) \cdot (cos\theta_{l+3} sin\theta_{m+3}) \tag{5.11}$$

and

$$0 <= \theta_{k+3} = tan^{-1}(y_k - y_l)/(x_k - x_l) < \pi \tag{5.12}$$

where subscript $n+3, n = k, l, m$ means the midpoints of the nodes, i.e. point 4,5 and 6 in . And k, l, m goes modulo 3 arround the the edges. Thus the expansion of

the transverse components ϕ_x, ϕ_y and the axial component ϕ_z in each element could be concluded as equation (5.13)

$$\Phi = \begin{pmatrix} \phi_x \\ \phi_y \\ \phi_z \end{pmatrix} = \begin{pmatrix} U^T\phi_{te} \\ V^T\phi_{te} \\ jN^T\phi_{te} \end{pmatrix} \tag{5.13}$$

One of the two drawbacks of nodal vectorial FEM is the difficulty to set boundary conditions because a boundary normal has to be defined. In this edge-based FEM, however, since both ϕ_z and ϕ_t are tangential to material interfaces, the tangential continuity can be straight forwardly imposed.

5.2.4 Finite Element Matrix

Substituting equation (5.13) into equation (5.1), equation (5.14) could be obtain

$$[K]\Phi - k_0^2[M]\Phi = 0 \tag{5.14}$$

with

$$[K] = \begin{pmatrix} [K_{tt}] & [K_{tz}] \\ K_{zt} & [K_{zz}] \end{pmatrix} \tag{5.15}$$

$$[M] = \begin{pmatrix} [M_{tt}] & 0 \\ 0 & [M_{zz}] \end{pmatrix} \tag{5.16}$$

where

$$[K_{tt}] = \sum_e \iint_e [p_x\beta^2 VV^T + p_y\beta^2 UU^T + 4p_z U_y U_y^T]dxdy \tag{5.17}$$

$$[K_{tz}] = [K_{tz}]^T = \sum_e \iint_e [p_x\beta V N_y^T + p_y\beta U N_x^T]dxdy \tag{5.18}$$

$$[K_{zz}] = \sum_e \iint_e [p_x N_y N_y^T + p_y N_x N_x^T]dxdy \tag{5.19}$$

$$[M_{tt}] = \sum_e \iint_e [q_x UU^T + q_y VV^T]dxdy \tag{5.20}$$

$$[M_{zz}] = \sum_e \iint_e q_x NN^T dxdy \tag{5.21}$$

where $W_\delta = \partial W/\partial\delta, W = U, V, N, \delta = x, y$ and the intergrals are as follows

$$\begin{aligned}[\iint_e UU^T dxdy]_{kl} &= A_e\tilde{a}_k\tilde{a}_l + A_e y_c(\tilde{a}_k\tilde{c}_l + \tilde{c}_k\tilde{a}_l) \\ &\quad + A_e\tilde{c}_k\tilde{c}_l(y_1^2 + y_2^2 + y_3^2 + 9y_c^2)/12\end{aligned} \tag{5.22}$$

$$\begin{aligned}[\iint_e VV^T dxdy]_{kl} &= A_e\tilde{b}_k\tilde{b}_l - A_e x_c(\tilde{b}_k\tilde{c}_l + \tilde{c}_k\tilde{b}_l) \\ &\quad + A_e\tilde{c}_k\tilde{c}_l(x_1^2 + x_2^2 + x_3^2 + 9x_c^2/12\end{aligned} \tag{5.23}$$

$$\begin{aligned}[\iint_e U_y U_y^T dxdy]_{kl} &= [\iint_e V_x V_x^T dxdy]_{kl} \\ &= -[\iint_e U_y V_x^T dxdy]_{kl} \\ &= -[\iint_e V_x U_y^T dxdy]_{kl} \\ &= A_e\tilde{c}_k\tilde{c}_l\end{aligned} \tag{5.24}$$

$$[\iint_e UN_x^T dxdy]_{kl} = (\tilde{a}_k + \tilde{c}_k y_c)b_l \tag{5.25}$$

$$[\iint_e VN_y^T dxdy]_{kl} = (\tilde{b}_k - \tilde{c}_k x_c)c_l \tag{5.26}$$

$$[\iint_e NN^T dxdy]_{kl} = A_e/12 + \delta_{ij}A_e/12 \qquad \delta_{ij} = 0, i \neq j; \delta_{ij} = 1, i = j \tag{5.27}$$

$$[\iint_e N_x N_x^T dxdy]_{kl} = \frac{1}{4A_e} b_k b_l \tag{5.28}$$

$$[\iint_e N_y N_y^T dxdy]_{kl} = \frac{1}{4A_e} c_k c_l \tag{5.29}$$

with

$$x_c = (x_1 + x_2 + x_3)/3 \tag{5.30}$$

$$y_c = (y_1 + y_2 + y_3)/3 \tag{5.31}$$

where all the intergrals are 3 by 3 matrix with subscript kl indicating the (k,l) element within the matrix.

5.3 Validation of Full Vectorial FEM with PRB Boundary Condition

5.3.1 Examples

In order to evaluate the performance of the Full Vectorial FEM, the same examples are used as in Scaler FEM Validation in Chapter 4. The modal analysis of a circular waveguide, a rectangular dielectric waveguide and a ridge waveguide is presented and

the effective refractive index are compared to both the scalar FEM and analytical values or the reference values (ridge waveguide) as shown in Table (5.1), Table (5.5) and Table (5.3).

Table 5.1: Effective Refractive index for the circular waveguide

	Vectorial FEM, PRB		
Mode Type	**609 nodes**	**1022 nodes**	**Analytical Values**
HE_{11}	2.268483	2.268515	2.268776
2nd	2.189032	2.194706	
3rd	2.186837	2.195157	

Note: H field is calculated.

Table 5.2: Effective refractive index of the fundamental quasi-TE mode for the ridge waveguide

	n_{eff}		Reference Values[2]
Mode Type	**VFEM**	**1300 nodes**	**VFEM**
t = 0.0 μm	3.1948536		3.1945511
t = 0.2 μm	3.1988334		3.1983379
t = 0.4 μm	3.2027885		3.2021418

Note: For purpose of comparison of published results in [2], with normalized frequency $b = \frac{n_{eff}^2 - n_s^2}{n_c^2 - n_s^2}$, we convert b in the paper to the n_{eff} shown in the table. H field is calculated. PRB boundary condition.

5.3.2 Orthogonality

In order to validate further for this Vectorial FEM, the orthogonality of the guided, box, and evanescent modes are shown in this section. As the definition in chapter 4

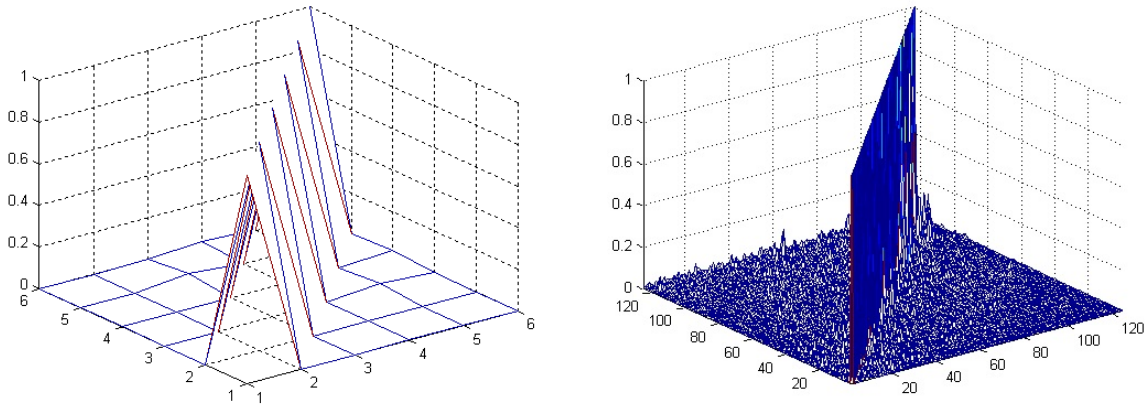

(a) Within guided modes (b) All modes

Figure 5.2: Mode orthogonality of the buried waveguide

Equation (4.29), the orthogonality of the all modes, including guided and box modes, are ensured in the Full Vectorial FEM as we could see from Figure (5.2). Please note that $\vec{E}_t$ and $\vec{H}_t$ are coupled to each other as Equation (2.13) and (2.14) shows. And it is easy to find out from the results and the reference paper that calculating by E field is not as accurate as H field. Thus in the following section, $\vec{E}_t$ is calculated from $\vec{H}_t$.

5.4 Validation of Full Vectorial FEM with PML and PRB Boundary Condition

We use the same PML scheme as in Figure (4.17) and coordinate-stretching factor in Formula (4.27). In this chapter, we are going to explore the complex mode rather than just the accuracy of the method.

5.4.1 Examples

Examples of a circular waveguide, ridge waveguide and buried waveguide are presented and characteristics explored in the following section.

Table (5.5) is the results of same structure of a circular waveguide in Figure (4.17). Selected mode profiles, one guided mode and one leaky mode is shown in Figure (5.3).

Table (5.6) is the results of same structure of a ridge waveguide in Figure (4.19) and Table (5.7) buried waveguide in Figure (4.9).

Table 5.3: Effective Refractive index of the step-index circular waveguide

	Simulated n_{eff}, 1022 nodes		
Mode Type	**VFEM PML**	**VFEM PRB**	**Analytical Values**
HE_{11}	2.268515-1.02e-8i	2.268515	2.268776
2nd	2.195264-8.61e-4i	2.194706	
3rd	2.189565-2.55e-3i	2.195157	

Note: H field is calculated. $R_{PML} = 10^{-3}$, $d_{PML} = 0.4 \times 10^{-6}$

5.4.2 Orthogonality

The orthogonality characteristics of a buried waveguide is shown in this section. Figure (5.4) is the inner production defined in Equation (4.29) between each modes.

5.5 Discussion

It is obvious that the performance of Vectorial FEM is much more better than Scalar FEM. And the PML boundary condition increases the accuracy compared with PRB boundary condition especially on higher order modes.

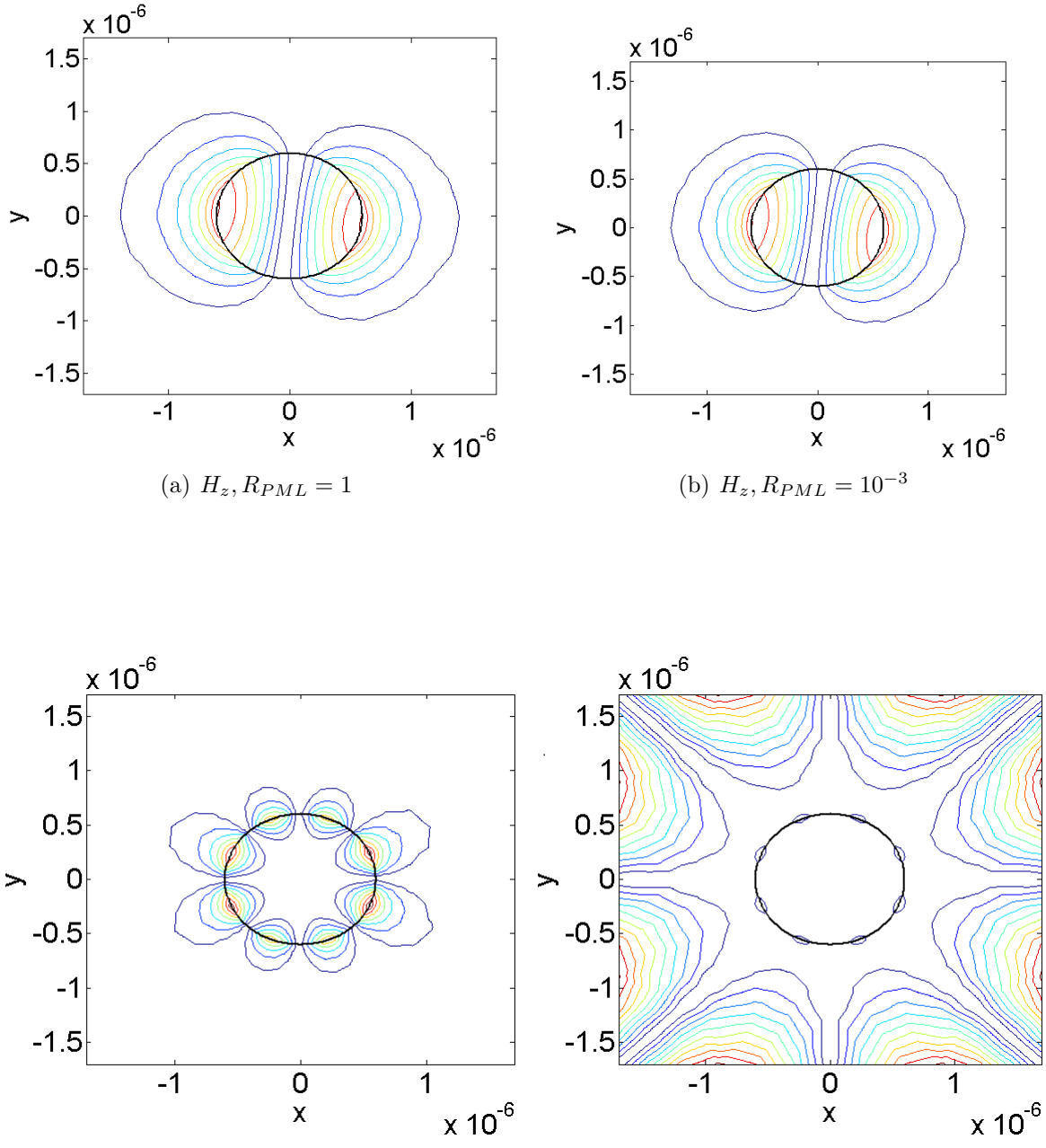

(a) $H_z, R_{PML} = 1$ (b) $H_z, R_{PML} = 10^{-3}$

(c) $H_z, R_{PML} = 1$ (d) $H_z, R_{PML} = 10^{-3}$

Figure 5.3: (a)(b) fundamental mode (HE11) profiles (c)(d) 3rd mode profiles of the circular waveguide

Table 5.4: Effective refractive index of a ridge waveguide

	Simulated (n_{eff}, 1300 nodes)		Reference Values[2]
Mode Type	**VFEM PML**	**VFEM PRB**	**VFEM**
t = 0.0 μm	3.1948112-1.53e-4i	3.1948536	3.1945511
2nd	3.1862457+3.75e-5i		
3rd	3.1603734-2.92e-3i		
4th	3.1542455-3.78e-3i		
t = 0.2 μm	3.1987257-5.92e-4i	3.1988334	3.1983379
2nd	3.1908089-1.80e-5i		
3rd	3.1798299-6.62e-3i		
4th	3.1664520-2.12e-3i		
5th	3.1535007-8.66e-3i		
t = 0.4 μm	3.2010806-1.28e-3i	3.2027885	3.2021418
2nd	3.1931707-3.34e-4i		
3rd	3.1864368-6.32e-3i		
4th	3.1746380-4.44e-3i		
5th	3.1513228-1.08e-3i		

Note: For purpose of comparison of published results in [2], with normalized frequency $b = \frac{n_{eff}^2 - n_s^2}{n_c^2 - n_s^2}$, we convert b in the paper to the n_{eff} shown in the table. H field is calculated.

Table 5.5: Effective refractive index of the buried waveguide

	Simulated n_{eff}, 899 nodes	
Mode Type	**VFEM PML**	**VFEM PRB**
1st	3.4303519-7.12e-4i	3.4304140
2nd	3.4289856+4.30e-4i	3.4287722
3rd	3.2816529-8.80e-3i	3.2812465
4th	3.2809211+1.54e-3i	3.2804437
5th	3.2737933 +7.45e-3i	3.2701605
6th	3.2711433-2.13e-3i	3.2674448
7th	3.1523069-1.67e-2i	
8th	3.1498120-1.86e-2i	
9th	3.1345361-1.55e-2i	

Note: H field is calculated. $R_{PML} = 10^{-3}$.

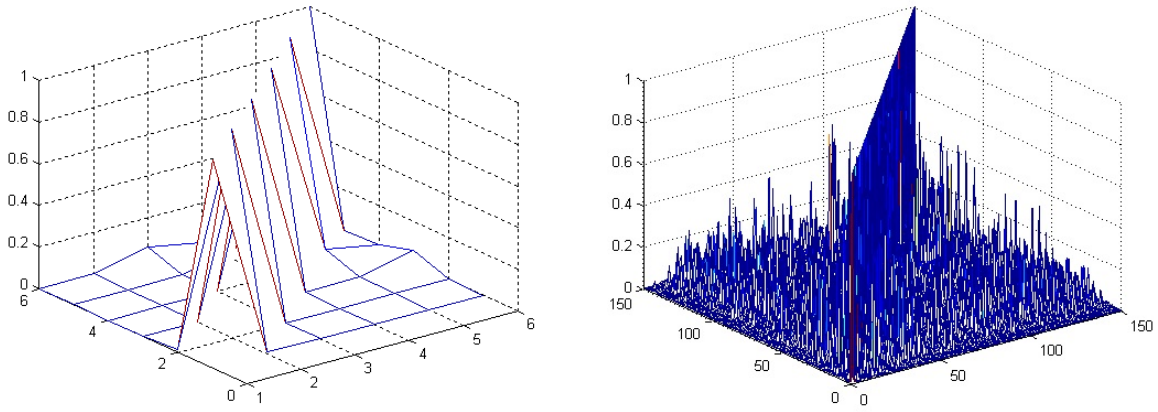

(a) Within guided modes (b) All modes

Figure 5.4: Complex mode orthogonality of the buried waveguide

With PRB boundary condition, the orthogonality between each modes is obviously good. However, in PML and PRB scheme, the orthogonality is good within guided modes but has error on higher order modes. One of the reason might be that the mesh size is not small enough. Compared with PRB BC, PML BC need a finer mesh within the PML region because the equivalent effective index is relatively high in PML region which means a high-contrast refractive index. Energy of higher modes is constrained in the PML region (such as the PML modes). With the same mesh but larger energy constrained, the error becomes larger.

So smaller grid and higher order algorithm are needed. However, as a frequency domain technique, the memory required is very large, which limits a finer mesh. The order of this algorithm is low because it assumes that the tangential component is constant along the element edge. Higher order FEM can be obtained if we set the tangential component changing linearly on a compromise of a larger dimension of the eigen matrix by Koshiba's method in [10].

Bibliography

[1] D. S. Burnett, *Finite Element Analysis*. Addison-Wesley Publishing Company, 1987.

[2] G. I and C. 216, "Comparison of different modelling techniques for longitudinally invariant integrated optical waveguides," *IEE Proceedings*, vol. 136, October 1989.

[3] J. Jin, *The Finite Element Method in electromagnetic*. John Wiley & Sons, Inc., 2 ed., 2002.

[4] J.-P. Berenger, "A Perfectly Matched Layer for the Absorption of Electromagnetic Waves," *Journal of Computational Physics*, vol. 114, pp. 185–200, 1994.

[5] W. C. Chew and W. H. Weedon, "A 3-D Perfectly Matched Medium From Modified Maxwells Equations with Stretched Coordinates," *Microwave Optical Technology Letter*, vol. 7, no. 13, pp. 599–604, 1994.

[6] S. G. Mikhlin, *Variational Methods in Mathematical Physics*. Pergamon Press: Distributed by Macmillan, New York, 2 ed., 1964.

[7] K. Okamoto, *Fundamentals of Optical Waveguides*. Elsevier Inc., 2 ed., 2006.

[8] J. Mu and W. P. Huang, "Simulation of Three-Dimensional Waveguide Discontinuities by a Full-Vector Mode-Matching Method Based on Finite-Difference Schemes," *Optics Express*, vol. 16, no. 22, 2008.

[9] A. Bossavit, "Solving Maxwell Equations in A Closed Cavity, and the Question of 'Spurious Modes'," *IEEE Tran. on Magnetics*, vol. 26, March 1990.

[10] M. Koshiba, "A Vector Finite Element Method With the High-Order Mixed-Interpolation-Type Triangular Elements for Optical Waveguiding Problems," *J. of Lightwave Technol.*, vol. 12, March 1994.

[11] M. Koshiba, "Simple and Efficient Finite-Element Analysis of Microwave and Optical Waveguides," *IEEE Tran. Microwave Theory Tech.*, vol. 40, February 1992.

[12] C. J. Reddy, M. D. Deshpande, C. R. Cockrell, and F. B. Beck, "Finite Element Method for Eigenvalue Problems in Electromagnetics," *NASA Technical Paper*, 1994.